NJC

Accepted Manuscript

This article can be cited before page numbers have been issued, to do this please use: S. S. Gurukar, V. Rajashekara shetty, R. Mariappa, M. M. Kittappa and D. H. Nagaraju, *New J. Chem.*, 2015, DOI: 10.1039/C5NJ01300C.

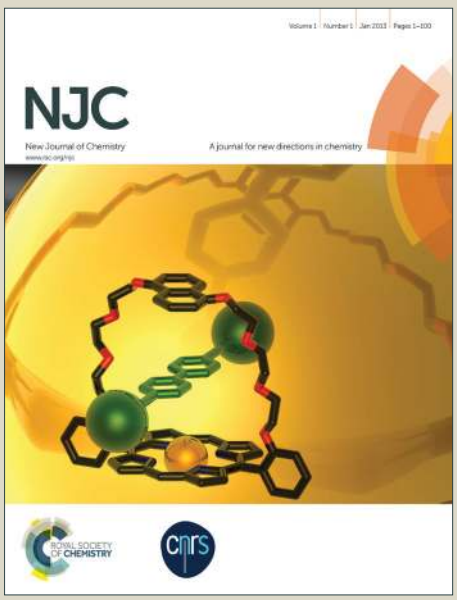

ROYAL SOCIETY OF CHEMISTRY

www.rsc.org/njc

View Article Online
DOI: 10.1039/C5NJ01300C

Novel synthetic approach for 1, 4-dihydroxyanthraquinone and the development of its Lithiated salts as anode material for aqueous rechargeable Lithium-ion batteries

Vijeth Rajshekar Shetty, Gurukar Shivappa Suresh, Marriappa Ramaiah, Kittappa Malavalli Mahadevan*, Doddahalli Hanumantharayudu Nagaraju.*

Vijeth R Shetty, G. S. Suresh*, M. Ramaiah
Department of Chemistry and Research Center,
NMKRV College for Women,
Jayanagar, Bangalore-560011, India
Telephone: 91-80-22443695
Fax no: 91-80-22440116
E-mail address: sureshssmrv@yahoo.co.in (G.S.Suresh)

Kittappa Malavalli Mahadevan*
PG-Center, Kuvempu University, Kadur-577548
Karnataka, India
E-mail address: mahadevan.kmm@gmail.com (K.M.Mahadevan)

Doddahalli Hanumantharayudu Nagaraju
King Abdullah University of Science and Technology
Thuwal, Kingdom of Saudi Arabia

View Article Online
DOI: 10.1039/C5NJ01300C

Abstract:

The influence of organic electrode materials in the field of lithium ion battery is becoming a keen interest for the present generation scientists. Here we are reporting a novel method of synthesis of electrode material by the combination of sono-chemical and thermal methods. The advantages of organic active material towards lithium ion battery are of core interest of this study. The structural confirmations are by FT-IR, ^{1}H NMR, MALDI-TOF Mass Spectroscopy and powder XRD data. The electrochemical properties of Lithiated-1,4-dihydroxyanthraquinone were studied using electrochemical-techniques such as Cyclic Voltammetry, Galvanostatic Cyclic Potential Limitation and Potentiostatic Electrochemical Impedance Spectroscopy. The satisfactory results towards stability of active species in the aqueous media, reasonable discharge capacity with 0.9 V average voltages and agreeable cycling performance during charge-discharge process with reproducibility are achieved. For the construction of the full cell, the anode material was coupled with the $LiNi_{1/3}Co_{1/3}Mn_{1/3}O_2$ as a cathode material.

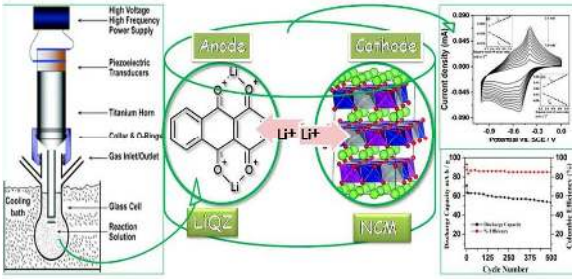

View Article Online
DOI: 10.1039/C5NJ01300C

Keywords: Aqueous rechargeable lithium batteries, Lithiated quinizarin, 1, 4-dihydroxyanthraquinone, Di-lithiated anthraquinone.

1. Introduction

According to the expectance of present generation towards portable electric devices, hybrid vehicles, bio-equipments with a prolonged lifetime operated by rechargeable battery system have commenced growth in the market. To fulfil such requirements of the present scenario, the development of energy storage devices acquire a major role. To overcome the energy crisis, the development of energy storage devices enlightens the lithium ion battery (LIB) resources as a powerful tool. By the utilization of existing aspects and development of new approaches in order to build up LIB technologies, current inventers looking forward for new ideas and contributing admirable requisites towards future generations. The methodological aspect such as aqueous and non-aqueous rechargeable lithium ion battery (RLIB) technology promises us towards the fulfilment of the needs of future generation energy storage devices. On this basis researchers have put forward their effort in the field of non-aqueous RLIB. The implementation of such field has its own way of developmental advantages but the drawbacks of these materials such as high cost; emission of CO_2 gas, natural hazards hinders the growth in materialization and their applications.[1] The electrochemical performance of few cathode materials such as $LiCoO_2$, $LiMn_2O_4$ and $Li[Ni_{1/3}Co_{1/3}Mn_{1/3}]O_2$ exhibits much better results aqueous media than in organic electrolytes.[2] They shows admirable charge rate performance like: a full charge can take less time than the time taken to fill a gasoline tank for traditional vehicles.[3] On the other hand, the low energy density due to the low electrochemical window of water, 1.229 V ascribes their main disadvantage over organic electrolyte.[2] Consequently, increasing the energy density of ARLBs has been a big challenge. To overcome such aspects the present research field has been extended to ARLB. The disadvantages linked with non-aqueous LIB by the use of high toxic and inflammable

View Article Online
DOI: 10.1039/C5NJ01300C

chemicals as organic solvents may be solved by using ARLBs. Many approaches have been made to progress the performance of the ARLIB as future energy storage devices.

In this regard, enormous efforts on the origin of ARLB were anticipated and have become one of the real energy sources for future generations.[4] The material usage for the electrode preparation mainly focused on inorganic composites, layered materials, organic moiety in inorganic voids as hybrid materials and organic aromatic compounds took a major role in electrochemical consideration. But proper utilization with respect to its availability, cost, eco friendliness and electro active properties, the organic electrode materials are becoming the keen interest nowadays. The influence of organic electrode materials in the field of lithium ion battery has becoming one of the boons for scientists. The usage of such low cost, eco-friendly, non toxic and naturally occurring organic compounds as electrode materials in aqueous rechargeable batteries boost the applications of LIB in electric and electronic devices as energy storage materials.

The main criteria for a good electroactive species for its pronounced electrochemical properties of organic species in battery application is the availability of active centres for redox process. In this regard naturally occurring compounds such as Ellagic acid a polyphenol from pomegranate husk, purpurin obtained from madder plant, dilithium rodizonate salt obtained from biomass[5-7] were used as active materials for non-aqueous RLIB. Indigo dye derivative such as 5, 7, 12, 14-pentacenetetrone are also used as energy storage cathode materials[8] in RLIB technology. It has been recognized that the molecules with hydroxyl, amine and carbonyl groups in conjugation with aromatic coordination serves as resourceful organic electrode materials. The anthraquinone moiety has the most versatile and useful redox-active C=O group, which serves as a good electrochemical activity in chemical and biological system.[9] The naturally occurring compounds such as polyphenol, anthracene, flavonoides, anthraquinone and their derivatives showing good electroactive

View Article Online
DOI: 10.1039/C5NJ01300C

properties, helps in their application strategies on RLIB. The scientific criteria towards the synthesis and application of organic energy storage materials mainly include two components. The first one is that the establishment of a new approach towards the synthesis and framework of organic molecules, which are electrochemically active; secondly the implementation of these materials in test cells to study its practical output for increased performance and evaluation. To carry out these objectives, the practical approach should be innovative, rapid, and efficient synthesis processes using economical and proper methods. The electroactivity of active centers get reduced or oxidized, which makes the organic salts to achieve an excellent electroactive species that tend to be an attractive tool in electrode materials. As per theoretical consideration a wide variety of single and multiple ring molecules, which could contain electrochemically active C=O functions shows enough capacities and ensure stability of the organic molecules in particular electrolytes.[7] The execution of ultra-sound in organic synthesis proves high yield when compared with other methods[10] This new way has been influencing not only on the practical yield, but also purity of the product. According to the RLIB concern, electrode materials have to be a highly pure and precise electroactive in nature to accomplish a good active material for electrochemical performance.

In this consideration, for the first time, we have proposed 9, 10-antharaquinone derivative such as quinizarin, as the organic electrode material for aqueous rechargeable lithium battery. The lithiation and de-lithiation in Li-ions are facilitated by the presence of carbonyl functional groups by means of redox reaction. The quinizarin moiety possesses two hydroxyl groups at alpha positions (1 and 4) of anthraquinone, which facilitates the system to show tautomeric conformation. The synthetic route that we proposed is a novel method for the synthesis of quinizarin. It involves a combination of sonochemistry and conventional thermal method, which is comparatively a better scheme as compared to microwave

View Article Online
DOI: 10.1039/C5NJ01300C

method [11] to obtain high yield and high purity. The lithiation of quinizarin was carried out in an inert atmosphere. The tautomeric conformational strategy of Lithiated compound was confirmed by both physical characterizations FT-IR, 1H-NMR, pXRD and electrochemical characterizations like CV, and Galvanostatic battery testing techniques and impedance measurements, which proves that the developed organic compound is act as one of the good anode material for aqueous RLIB technology. A Galvanostatic study shows a good discharge capacity of about 71 mA h g^{-1} with ~ 0.9 V average potential by coupling with $LiNi_{1/3}Co_{1/3}Mn_{1/3}O_2$ as cathode. Impedance measurement encountered a finite diffusion reveals that a near capacitive behaviour of the electrode material by the appearance of inclined lines at low frequency region.

2. Experimental Section

2.1.Materials and reagents

Chemicals and reagents which were used for our experiments, Phthalic anhydride, Boric acid, p-chlorophenol, Potassium hydroxide, LiOH, Polytetrafluroethylene powder (12 micron), N-methyl-2-pyrrolidone and lithium sulphate were procured from Sigma Aldrich. All other chemicals used were of analytical grade unless otherwise mentioned and used without further purification. All solutions for experiments were prepared by using pure water. Synthesis of quinizarin was done by using QSONICA Ultrasonic processor (20 KHz), annealing was carried out at 300 ºC in tubular furnace. FTIR studies were made by using Shimadzu instrument, ^{1}H NMR studies were made by using Bruker at 400 MHz processor, MALDI-TOF Mass Spectrometer by the use of HCT ultra ETD II and X-ray powder diffraction (XRD) using Philips X'pert Pro Diffractometer (Cu K radiation, secondary graphite monochromator) analytical instrument.

2.2. Scheme for synthesis

View Article Online
DOI: 10.1039/C5NJ01300C

The new synthetic approach of quinizarin was carried out by using finely powdered solid phthalic anhydride (2.0M), was sonicated in an acidic medium of concentrated sulphuric acid in the presence of catalytic amount of finely powdered boric acid, by using Ultrasonic processor at room temperature for 30 min. In that time intervals p-chlorophenol (0.9M) was added drop by drop for. The green colored reaction mixture obtained was subjected to refluxation for 30min at 60 ºC, a dark scarlet red colored melt was poured into ice cooled water with continuous stirring and the obtained compound was filtered. The precipitate was boiled with water and filtered hot to remove un-reacted phthalic anhydride. The residue was suspended in boiling water and to this sufficient quantity of 10N Potassium hydroxide was added until purple colored quinizarin solution was obtained. The alkali solution was filtered and hot water was used as washing solution. The alkali solution was acidified with 5% hydrochloric acid to liberate reddish-brown crystalline powder quinizarin. The reaction was monitored by thin layer chromatography (TLC) for the completion of reaction. A fraction of the sample was recrystallized with hexane which gave orange needle like crystals and melted at 200 ºC.[12] The synthetic route is as shown in scheme 1.

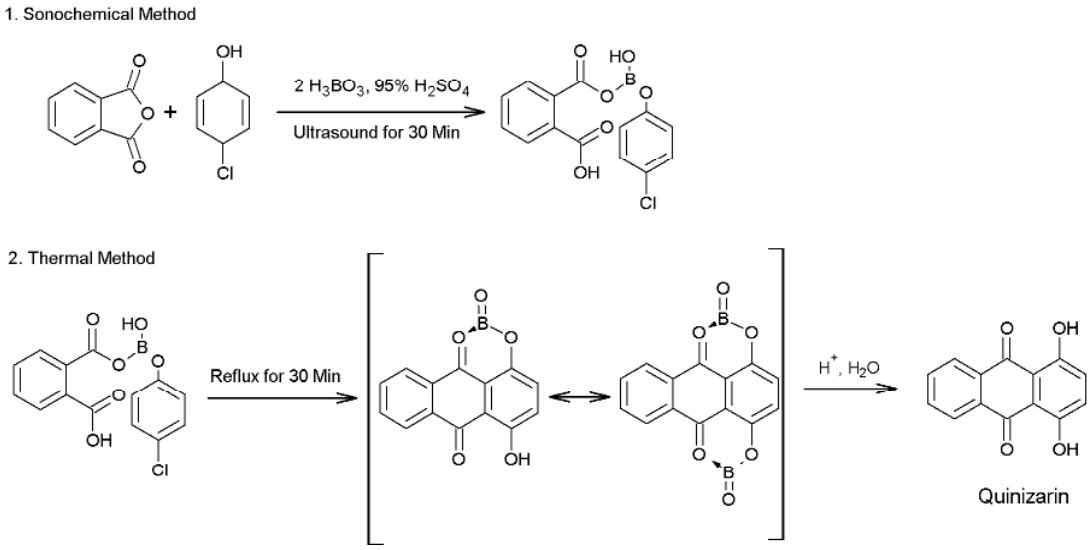

View Article Online
DOI: 10.1039/C5NJ01300C

Scheme 1**:** Synthetic route for 1, 4-dihydroxyanthraquinone by 1) Sonochemical method 2) thermal method

The lithiation of 1, 4-dihydroxyantraquinone was carried out in an inert atmosphere. The stoichiometric amount (0.75M) of 1, 4-DHAQ was dissolved in oxygen free ethyl alcohol to avoid oxidation of keto-enolic form of $C_{14}H_6O_4^{2-}$ anion. The alcoholic solution of quinizarin was heated to 60 ºC and this temperature was maintained till the completion of drop-wise addition of 1.5M/L of aqueous LiOH with constant stirring. Then temperature was increased to 80 ºC and maintained for 48 hours with continuous stirring. The progress and completion of the reaction was monitored by TLC. After the completion of the reaction, the flask was kept aside to allow the blue colored crystalline precipitate to settle at the bottom, which was later separated from alcohol by centrifugation. Blue crystalline precipitate was washed with cold distilled water and then dried in a vacuum oven for 12 hours at 80 ºC. The light blue colored fine powder obtained was then subjected for annealing under N_2 atmosphere up to three hours in a tubular furnace at 300 ºC. The fraction of the sample was recrystallized with charcoal using oxygen free ethyl alcohol.[13] Possible lithiation of quinizarin is depicted in scheme (2).

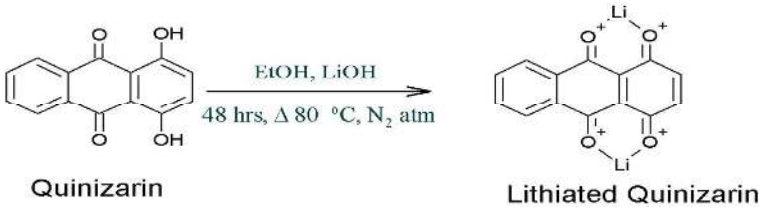

Scheme 2**:** Lithiation of quinizarin

For the electrochemical performance the working electrode was prepared by using a stainless steel mesh of 2.23 cm^2 geometric surface area which was cleaned to remove surface oxide layer by sand paper and washed with pure water and alcohol, which was used as

View Article Online
DOI: 10.1039/C5NJ01300C

current collector. The cleaned electrode was dried and weighed. $Li_2(C_{14}H_6O_4)$, carbon black and binder Polytetrafluroacetylene were mixed in the stoichiometric ratio of 80:10:10 and ground in a mortar. The slurry was prepared by adding a few drops of N-methyl-2-pyrrolidone [14] to the mixture. The previously weighed SS mesh was coated with slurry and dried at 80 ºC for 10 hours under vacuum. The electrochemical measurements were carried out in an aqueous electrolyte such as saturated Li_2SO_4 solution medium with Pt counter electrode and saturated calomel electrode as the reference electrode. The solubility of electrode materials in saturated electrolyte was studied under temperature treatment by placing the electrode in electrolyte medium for 48 hours at 50 °C and 60 °C. There was no changes observed in active mass at 50 °C but a 20% weight loss was observed under 60 °C after 48 hours.

The synthesis of nano-sized $LiMn_{1/3}Ni_{1/3}Co_{1/3}O_2$ was done by material by RAPET method, which was used as cathode. The fabrication of cathode material was done by using 80:10:10 (active material: carbon black: PTFE) were grained and a slurry was prepared by NMP and applied on 12 mm diameter SS mesh electrode. Before coupling with anode, the cathode was dried at 85 ^{0}C in a vaccume oven for 10 hrs. The stability of cathode material towards the saturated electrolyte was determined by temperature treatment. We have proved that the active material was stable enough in the aqueous medium at different temperatures. As the temperature increases to 70 °C dissolution was observed up to 25 to 30 %. Apart from solubility factors, the stability parameters like thermal stability, columbic efficiency with cycling capability in aqueous media for NCM active material was reported elsewhere [15] by our research group.

2.3. Construction of cell for electrochemical performance

The cell was constructed by using an aqueous saturated solution of 10 ml Li_2SO_4 as electrolyte in a cylindrical glass container. The CV and EIS studies were examined in a three

View Article Online
DOI: 10.1039/C5NJ01300C

electrode system containing LiQZ as a working, Pt foil as counter and SCE as reference electrode. Whereas, in GCPL studies $LiNi_{1/3}Co_{1/3}Mn_{1/3}O_2$ used as cathode.

3. Result and discussion

3.1. Spectral details

An organic moiety derived from anthraquinone called quinizarin was introduced to ARLB as an electrode material in the present work. The presence of hydroxy functional groups preferably enhances the electrochemical activity towards the battery performance in the Lithiated form. The keto-enolate forms of the active species play a significant role in the preferential application of these materials in ARLB. The synthesis of quinizarin was achieved by a novel method in which the powdered form of phthalic anhydride, boric acid were mixed and sonicated in concentrated sulphuric acid medium followed by heat treatment with reflux process. For the electrochemical studies the primary compound quinizarin was subjected to lithiation under nitrogen atmosphere. The recovery of the products quinizarin and Lithiated quinizarin were done as detailed in section 2.2. The structure of both quinizarin and Lithiated quinizarin was confirmed by FT-IR, ^{1}H-NMR, MALDI-TOF MS, and pXRD techniques. Fig. 1A shows the FT-IR spectra of the quinizarin with a broad band at the vicinity of 3450 cm^{-1} predicts the intermolecular hydrogen bonds which confirm the tautomerisation. In addition, the absorption peak at 1638 cm^{-1} is due to stretching vibration of C=O bonds of the enolate form of quinizarin which facilitate the lithiation in tautomeric conformation and which has been confirmed by the shifting of peaks towards lower wave number with reduced intensity. The Fig. 1B predict the proton NMR data of quinizarin are (400 MHz, DMSO) δ 12.695 (2H, s), 8.246-8.291 (2H, m), 7.955-8.001 (2H, m), 7.439 (2H, s), which emphasises a characteristic multiplet for antharaquinone at the vicsinity of 8.246-8.291 ppm chemical shift value. A singlet at 12.965 ppm reaveals the phenolic proton of anthraquinone. In mass

View Article Online
DOI: 10.1039/C5NJ01300C

spectral data of quinizarin in (C), a peak appeared at 241.808 *m/z* value in the form of $[M+H]^+$ molecular ion peak, which render for the presence of tautomeric conformation. Whereas, in case of Lithiated compound in (A) the FT-IR spectra confirms that the lithiation has been occurred at the position of hydrogen in the form of tautomerisation with carbonyl group. This can be attributed by the reduced absorbance band at the vicinity of 3450 cm^{-1}, shifting of C=O and C=C absorption bands towards the lower wavenumber. The aromatic C=C stretching vibration at 1523 cm^{-1} [16] in both cases reveals anthraquinone characteristics. The ^1H NMR data of Lithiated quinizarin in (B)**:** ^1H NMR (400 MHz, DMSO) δ 8.283 (2H, b), 7.850 (2H, b), 7.114 (2H, b). The disapperence of a peak at 12.965 ppm indicate the lithiation of quinizarin at the position of –OH. The intensity of peakes at 8.246-8.291 ppm values have been reduced may be due to the metalation effect. Due to the presence of metal moity in the position of proton reduces coupling constants and sensitivity towards proton NMR. From the mass spectral details, it is clear that a molecular ion peak at 252.201 *m/z* value for Lithiated quinizarin (C) in $[M+H]^+$ form reveals that two lithium ions have been substituted in the position of hydrogen. Powder X-ray diffraction analysis of quinizarin and Lithiated quinizarin were carried out to evaluate their crystalline states, shown in Fig. 1D. From the pXRD profile, a strong diffraction peaks indexed by monoclinic structure due to its π-π stacking flanked by the anthraquinone ring layers[9] similar to that of the pXRD profile of anthraquinone. The diffraction peak intensity of Lithiated compound gradually decreases and the line broadening increases due to metal-carbonyl group interaction.

The spectral details were commencing the structural confirmation of both quinizarin and its Lithiated forms. The lithiation of quinizarin will take place as shown in scheme 2 which indicates the strong OH bonding that hinders the lithiation at 1 and 4 position so that the keto-enolic form of lithiation was favourable which imparted to tautomeric conformation. From above observations the lithiation has been occurred by means of tautomeric

View Article Online
DOI: 10.1039/C5NJ01300C

conformation, which facilitates the lithiation/de-lithiation during electrochemical activity by redox process. Scheme 3 shows possible redox reaction occurred during electrochemical performance.

Overall cell performance:

During Charge:

At anode: $Li_x(C_{14}H_6O_4) + e^- + Li^+ \longrightarrow Li_{x+1}(C_{14}H_6O_4)$

At cathode: $Li_yNi_{1/3}Co_{1/3}Mn_{1/3}O_2 \longrightarrow Li_{y-1}Ni_{1/3}Co_{1/3}Mn_{1/3}O_2 + e^- + Li^+$

During dis-charge:

At anode: $Li_{x+1}(C_{14}H_6O_4) \longrightarrow Li_x(C_{14}H_6O_4) + e^- + Li^+$

At cathode: $Li_{y-1}Ni_{1/3}Co_{1/3}Mn_{1/3}O_2 + e^- + Li^+ \longrightarrow Li_yNi_{1/3}Co_{1/3}Mn_{1/3}O_2$

Overall Cell Reaction:

$$Li_x(C_{14}H_6O_4) + Li_yNi_{1/3}Co_{1/3}Mn_{1/3}O_2 \underset{\text{Dis-Charge}}{\overset{\text{Charge}}{\rightleftharpoons}} Li_{x+1}(C_{14}H_6O_4) + Li_{y-1}Ni_{1/3}Co_{1/3}Mn_{1/3}O_2$$

Scheme 3*:* Electrochemical Lithiation/delithiation process of Lithiated quinizarin

3.2. Electrochemical performance

3.2.1. Cyclic voltammetric studies

The electrochemical characterizations of Lithiated quinizarin were performed by cyclic voltammetry, Galvanostatic charge/discharge method and Potentiostatic electrochemical impedance spectroscopy. Fig. 2a shows the CV of Li_2 ($C_{14}H_6O_4$) in saturated Li_2SO_4 solution recorded at a potential scan rate of 0.5 mV/s between the potential window of 0.2 V to -1.0 V. The CV depicts two oxidation peaks, a sharp peak at –0.39 V and a broad peak at -0.60 V during charging process which corresponds to the oxidation of anode material. During the first negtive sweep, two blent reduction peaks observed at the vicinity of -0.6 V is which get splits into two peaks at -0.53 V and -0.70 V. These two reduction peaks corresponds to two

View Article Online
DOI: 10.1039/C5NJ01300C

reduction process of anode material, which reveals that the redox process of keto-enolic form of Lithiated quinizarin in tautomeric conformation.[7]

From the CV profile it is clear that the appearance of broad peaks one in each during oxidation and reduction is may be due to partial inserstion/deinsertion of lithium ions. In the second negative sweep, feeble reduction peaks are observed accompanying with the transformation between two carbonyl groups and lithium ions , forming the lithium enolate form .[17] The CV profile at the potential scan rate of 0.5 mV s^{-1} shows no change in the shape and peak potentials, which means that the carbonyl group-enolate mutual transformation reaction is reversible.[16,18-20] As per the literature, the appearance of plateaus in CV curves are due to the phase transition phenomenon during electrochemical performance of the material.[21] But in the present work the cyclic voltammogram shows no platues which may be due to the redox property of the organic electrode materials. Herewith we can signify that, the LiQZ will not show any phasetransition phenomenon during redox reaction. This lithium organic co-ordination compound with carbonyl groups aid the formation of lithium enolate, which helps in insertion and deinsertion of lithium ions reversibly when the carbonyl group reduced or oxidised, which promises us to use this material as energy-storage system in Li-ion batteries. Both the anodic and cathodic peaks are at negative potential with high reversibility reveals that the active material can be desingned to use as an anode mateiral in LiB thechnology. The experimental results from CV Fig. 2a reveals, the sum of reductive current is greater than that of sum of oxidative current due to the greater diffusion of electroactive species under reductive potential. The first columbic efficiency of about 93% has been achieved during first insertion/de-insertion of Li^+ ion in CV experiments of electrode material, which has given similar results during charge/discharge by Galvanostatic studies performed in a three electrode system.

View Article Online
DOI: 10.1039/C5NJ01300C

According to theoritical perception, the potential separation between the peaks and the shape of a particular peak mainly depends on the partical size and applied scan rate. In homogeneous sized active materials of the electrode with smaller sized particals, during the potential scan from heigher to lower potentials, the CV peaks become sharper and narrower, which also shows that the potential diffrence between the peaks for insertion-deinsertion process become smaller.[18] This result corresponds with the CV profile obtained by different potential scan rates from 0.1 mV s^{-1} to 1.0 mV s^{-1} as in Fig. 2b, the change in shape of the CV curve with narrowing of peak can be observed from higher to lower potential scan rates with increase in peak current, I_c higher to lower potential scan rate. The inset of the Fig. 2b shows a linear relationship between I_p vs. $\sqrt{\upsilon}$ or υ, this explicitly proves that at lower potential scan rates the current is directly proportional to υ, while at higher potential scan rates the current is directly proportional to $\sqrt{\upsilon}$. This proves that the accumulation/consumption mechanism favours the slow scan rate, whereas at high scan rate semi-infinite diffusion is valid.[18] At different potential scan rate CV, at a constant potential showed a linear positive increase in the current during charging and linear negative increase during discharge, which indicates the reversibility in the carbonyl group-enolate mutual transformation reaction. Such a mutual transformation reaction frequently referred to as reversible electron transfer reactions. The peak current for a reversible couple at 25 ºC is given by the Randles-Sevcik equation as given below,

$$i_p = (2.69 \text{ X } 10^5)\, n^{3/2}\, \text{ACD}^{1/2}\, \upsilon$$

where, i_p is the peak current, n is the number of electrons involved in charge transfer reaction, A is the area of the electrode in cm^2, C is the concentration in mol/dm^3, D is diffusion co-efficient in cm^2 / s and υ scan rate in mV / s. The inset of Fig. 2b for linear graph of curve fitting indicates that the current is directly proportional to the square root of the scan rate which can be attributed to the reversible electron transfer reactions. The formal potential of

View Article Online
DOI: 10.1039/C5NJ01300C

anode material calculated using $E^{\circ} = (E_{pa} + E_{pc)} / 2$ and peak potential separation (ΔE) for the reversible system (given by the Nernst equation; $\Delta E_p = E_{pa} - E_{pc}$) are found to be 0.0295 and 0.148 V respectively. Fig. 2c shows the effect of slow scan rate (at 0.05 mVs^{-1}) on CV profile, which reveals that high reversible insertion/deinsertion of lithium ion during oxidation and reduction of anode material respectively.

3.2.2. Galvanostatic charge-discharge studies

Galvanostatic charge/discharge curve of $LiNi_{1/3}Co_{1/3}Mn_{1/3}O_2$ / $Li_X(C_{14}H_6O_4$ cell at C/10 rate performed between -1.0 V to 1.3 V and the discharge capacity was found to be about 71 mAh g^{-1}as shown in the Fig. 3a. The potential window -1.0 V to 1.3 V for such cell with $LiNi_{1/3}Co_{1/3}Mn_{1/3}O_2$ cathode material was used by H.Wang et al.[22] Fig. 2d shows that, the evolution of oxygen was took place at 1.32 volts for stain less steel mesh electrode in saturated Li_2SO_4 aqueous solution. This O_2 overpotential may be because of saturated condition of electrolyte. The electrochemical performance of the cell was studied at 0.05 mA current. The possible electrochemical performance of cell is as shown in Scheme 3.

The π-π staking interaction of molecules, the existence of partial lithiation is possible. This was also predicted by the fig. 3d for the x(Li^+) ion insertion/deinsertion verses applied potential for both charge and discharge is of 0.8, which reveals that approximately one Li+ insertion/deinsertion may takes place with cathode material as predicted in above equation. During discharge at – 0.665 V one Li+ ion insertion and at 0.96 V deinsertion of one Li+ ion on $Li_X(C_{14}H_6O_4)$ anode material takes place respectively. The active mass of the anode and cathode were calculated by the ratio of specific capacities of the electrode materials as 278 mAh g^{-1} of cathode and 213 mAh g^{-1} anodes. The first discharge capacity is of 71 mA h g^{-1} was obtained which is based on the weight of both anode and cathode in the ratio 1:0.75 respectively.

View Article Online
DOI: 10.1039/C5NJ01300C

The first columbic efficiency was calculated for first Galvanostatic charge/discharge processes by the consideration of n/p ratio of active materials was about 93% as in case of CV studies, which reveals that the cell performance was mainly regulated by means of redox process of negative material. The $LiNi_{1/3}Co_{1/3}Mn_{1/3}O_2$ as cathode coupled with our working electrode provides a source of Li ion during cell performance.

The comparative studies by GCPL at different n/p ratio of electrode materials reveals that the effective columbic efficiency of about 93% was obtained at the ratio 1:0.75, which shows a good reversible mechanism of lithiation/delithiation at C/10 rate. Whereas other profiles for different n/p ratios such as 1: 0.5, 1:1 and 0.75: 1 as shown in fig. 4 b, c and d have given 80%, 84% and 47% columbic efficiency respectively. The agreeable result was obtained by to 1:0.75 n/p ratio may be due to the proper mechanism of lithiation and delithiation during charge discharge process was occurred by redox reaction.

After first cycle the capacity suddenly decreased to 66 mAh g^{-1} which is attributed to the reduced particle size of anode material or due to the dissolution of active material into the electrolyte.[23, 24] Later the capacity remains almost the same of in the vicinity of 60 mAh g^{-1} with 90% columbic efficiency up to 500 cycles as shown in discharge capacity versus cycle number profile in Fig. 3c. Satisfactory columbic efficiency with number of cycles indicates the stability of the active material in aqueous system. About 10% irreversibility in the capacity loss is attributed because of different values of x. The inset of fig. 3d shows that the x value has been reduced to 0.6 for 2^{nd} cycle, which is one of the reasons for sudden decline in the discharge capacity in 2^{nd} cycle. The capacity fading from the cycle number 2 to 500 was negligible, which reveals that the stabilization of quinonyl forms of Lithiated quinizarin.[16] After second cycle onwards the discharge plateaus decline, charge plateaus incline this may be due to the increase in the polarization of the electrodes or the semi-infinite diffusion of lithium ion towards electrodes, as explained in CV measurements.

View Article Online
DOI: 10.1039/C5NJ01300C

The half cell potential determination is an essential criterion to formulate a cell. The electrochemical characterization of a particular type of electroactive material by three electrode system, under an applied potential provide a CV profile, whereas under applied predetermined current, the cell system gives a charge discharge profile. The significant correlation of commercial product depends on the average potential of the cell. In this regard, we were subjected both the electrodes to charge discharge performance by taking large Pt foil as counter electrode and SCE coupled with anode/cathode in saturated Li_2SO_4 solution. From the fig. 5. it has been shown that, the charge discharge cycles at C/8 rate gave the anodic (5a) and cathodic (5b) half cell potentials of – 0.201 V and + 0.699 V respectively. The average cell potential of 0.9 V was obtained by the cell formulation LiQZ | Aq. Saturated Li_2SO_4| NCM system. This shows that output voltage of the LiQZ | Aq. saturated Li_2SO_4 | NCM cell is comparable to those of Ni- MH and Ni-Cd cells (1.2 V).[13] In fact the capacity is greater than that of Ni-Cd cells (40 – 50 mAh g^{-1}) and it is possible to reach the capacity level of Ni-MH systems (≈200 mAh g^{-1}) by further studies.

In case of the GCPL profile of primary lithium and Ni-MH batteries the appearance of knee point reveals a sudden drop off in the voltage.[25] Whereas, LiQZ | Aq. saturated Li_2SO_4| NCM system shows horizontally declining discharge profile, which promotes large number of cycling capability with considerable discharge efficiency.

In case of inorganic layered material usually it is observed that the variation in the polarization between charge/discharge curves due to irreversible capacity loss,[16] which is because of irreversible doping of lithium ions in the material. Such materials also show the increase in polarization of charge/discharge curves due to the formation of an undesired SEI layer caused by the electrode and electrolyte side reaction.[16] But in case of organic active materials the structural variation, pulverization of active material with increase in cycle number and low stability of active material towards electrolyte commence a major effect for

View Article Online
DOI: 10.1039/C5NJ01300C

sudden capacity loss.[26] The capacity of keto-enolate electrode material at different charge/discharge rates such as from C/8 to C/1 show the stability of electrode material as shown in the Fig. 3b.

3.2.3. Potentiostatic Electrochemical Impedance Spectroscopic studies

The impedance measurement with an open-circuit potential -0.201 V for anodic fresh electrode in three electrode system reveals that a depressed semicircle in the high-frequency region and a linear portion at low frequency region which is a characteristic semi-infinite diffusion of lithium ions.[14] The appearance of semicircle at high frequency region is due to the charge transfer reaction between surface film and the electrode, which is one of the common phenomenon in case of non-aqueous RLIB. There are two instances for the non-existence of SEI layer. The first one, in aqueous electrolyte medium if there is a formation of SEI, the layer will be of very thin and offers minor resistance.[27] and which may be due to the Li^+ ion migration through surface passivating layer.[28] The second one is, in organic electrode materials, the semi-infinite diffusion is favourable during lithiation and delithiation process. From the fig. 6a to d it is clear that the Nyquist family plots after cycling processes shows prominent Warburg impedances without except for fresh electrode. The appearance of Warburg lines with a slope greater than an angle of 45˚ shows a near capacitive behaviour with a mass transport of active material due to finite diffusion on inhomogeneous distribution of electro-active species. This is because of more than one electrochemical processes are drawn-out in active species and involved more than one electron transfer processes, which shows great variation in R_{ct} values. On the other hand it is also be due to the capacitor in the circuit which acts like CPE or it can be due to mass transport effect.[14] Here, it is relevant that the replacement of capacitor by constant phase element (CPE, Q), which is an imperfect capacitor. As per the experimental result obtained from the EIS, the existence of low

View Article Online
DOI: 10.1039/C5NJ01300C

frequency diagonal line shows imperfect capacitor behaviour. Such effects may be due the porosity or roughness of the electrode material surface.[29]

The experimental impedance spectra were fitted by using the equivalent circuit as shown in the Fig. 6e. According to this circuit arrangement, R_S is the solution resistance, R_{ct} is corresponds to medium frequency resistance of the charge transfer between the surface film and solution, which is due to diffusion by redox process in enolate conformation, R_f is the resistance for Li^+ migration through the surface film, the Warburg impedance, Z_W corresponds to lithium ion diffusion in the bulk particles, C_{dl} double layer capacitance and Q is constant phase element. Where capacitor in circuit **e** was replaced by CPE, in which R_{ct} and Q parallel circuit that indicates the presence of thin surface film layer on the electrode [29, 30]. The equivalent circuit is divided into three parts which emphasis (i) solution resistance at higher frequency region, (ii) R-Q parallel circuit for CPE and (iii) charge transfer resistance with Warburg diffusion term in low frequency region appears as a diagonal line with an angle slightly greater than 45° shows a near capacitive behaviour, which vague the semicircles shows finite diffusion.

Nyquist measurements support the redox reaction of Keto-enolate form of Lithiated quinizarin by the interaction with solution species and the electrode material. Fresh surface shows a large semicircle throughout the impedance measurement, but after first cycle the change in shape of the curve is due to slow charge transfer process with constant electrolyte resistance attributed as a result of simulation table of impedance spectra indicating the partial lithiation/delithiation process.

The kinetic parameters were plotted against number of cyclic performances shown in fig. 7 a to c, which reveals that the capacitance and charge transfer resistance were constant as there was no change in impedance measurements. This emphasis that the stable keto-

View Article Online
DOI: 10.1039/C5NJ01300C

enolate conformation of Lithiated quinizarin substantially a good anode material for aqueous rechargeable lithium ion battery. As per the stability concern the active material is extensively stable in aqueous medium even after 250th cycle during impedance measurement.

4. Conclusion:

By summarizing, the synthetic route that we proposed is not only reducing the time consumption for the completion of the reaction compared with other schemes, but also improves the quality and yield of the product. The combination of Ultrasound and thermal methods for the synthesis of quinizarin has become the best approach to fulfil the needs of rechargeable lithium ion battery performance. The structure and composition of quinizarin and Lithiated quinizarin were confirmed by preliminary tests, elemental analysis and spectral details. The electrochemical performance signifies that the stability of electrode materials in saturated media in particular potential window of water. The reversible lithiation/de-lithiation process was predicted in cyclic voltammetric performance confirms the keto-enolate conformation, which also proves that the semi-infinite diffusion of Li^+ ion during charge/discharge process. The Galvanostatic charge/discharge performance at C/10 rate favoured towards good cycling behaviour with appreciable discharge capacity for aqueous system. The sudden decline in the discharge capacity from first cycle to second cycle was due to polarization of electrode material or semi-infinite diffusion or could be due to the pulverization of active material. In comparison with charge/discharge profile of Ni-MH batteries, present system shows a steady decrease in the discharge capacity, large number of cycling capability with considerable efficiency. This shows an output voltage of ~0.9 V comparable to those of Ni- MH and Ni-Cd cells (1.2 V). Nyquist family reveals that, the appearance of prominent Warburg lines throughout the spectral measurements was due to finite to semi-infinite diffusion of Li^+ ions in an inhomogenously distributed electrode material on current collector surface, which shows a near capacitor behaviour.

View Article Online
DOI: 10.1039/C5NJ01300C

Electrochemical performance of the system confirms that Lithiated quinizarin is one of the good electrode materials for aqueous rechargeable lithium ion battery. Its further implementation in non-aqueous rechargeable system also contributes in the betterment of lithium ion battery technology.

Author contributions

The manuscript was written through contributions of all authors. All authors have given approval to the final version of the manuscript.

Acknowledgments

The authors gratefully acknowledge the financial support from Science and Engineering Research Board, Department of Science and Technology, New Delhi. We thank Sri.A.V.S.Murthy, Honorary secretary, Rashtreeya Sikshana Samiti Trust, Bangalore and Dr. Snehalata G. Nadiger, Principal, NMKRV College for Women, Bangalore for their continuous support and encouragement.

References

1 H.Chen, P. Poizot, F. Dolhem, N. I. Basir, O. Mentre and J. M. Tarascon, *Electrochemical and Solid-State Letters,* 2009, **12**, A102.

2 F. X. Wang, S. Y. Xiao, Z. Chang, Y. Q. Yang and Y. P. Wu, *Chem. Commun*., 2013, **49**, 9209

3 Y. Hou, X. Wang, Y. Zhu, C. Hu, Z. Chang, Y. Wu, R. Holze, *J. Mater. Chem. A*, 2013, **1**, 14713.

4 K. C. Mahesh, H. Manjunatha, T. V. Venkatesha, G.S.Suresh, *J Solid State Electrochem*, 2012, **16**, 3559.

5 A. L. M. Reddy, S. Nagarajan, P. Chumyim, S. R. Gowda, P. Pradhan, S. R. Jadhav, M. Dubey, G. John and P. M. Ajayan, *Sci.Rep.,* 2012, **2**, 960.

View Article Online
DOI: 10.1039/C5NJ01300C

6 M. Yao, M. Araki, Hiroshi Senoh, Shin-ichi Yamazaki, Tetsuo Sakai, and Kazuaki Yasuda, *Chem. Lett*., 2010, **39**, 950.

7 V. Y. Fain, B. E. Zaitsev, M. A. Ryabov, *Russian Journal of Organic Chemistry*, 2006, **42**, 1464.

8 M. Yao, H. Senoh, T. Sakai and T. Kiyobayashi, *Int. J. Electrochem. Sci.,* 2011, **6**, 2905 - 2911.

9 P. Bu, S. Liu, Y. Lu, S. Zhuang, H. Wang and F. Tu, *Int. J. Electrochem. Sci.,* 2012, **7**, 4617-4624.

10 H. Zang, M. Wang, B. W. Chang, J. Song, *Ultrasonics Sonochemistry* 2009, **16**, 301.

11 A. V. El'tsov, N. B. Sokolova, A. D. Grigor'ev, N. M. Dmitrieva, and A. S. Shtol'vin, *Russian Journal of General Chemistry*, 2002,**72**, 255.

12 J. M. Zheng, Z. R. Zhang, X. B. Wu, Z. X. Dong, Z. Zhu and Y. Yang, *J.Electrochem.Soc.,* 2008, **155**, A775.

13 R. Zeng, X. Li, Y. Qiu, W. Li, J. Yi, D. Lu, C. Tan, M. Xu, *Electrochemistry communications* 2010, **12**, 1253.

14 N. Maouche and B. Nessark, *Int. J. Electrochemistry.,* 2011, **1**.

15. K. C. Mahesh, H. Manjunatha, R. B. Shivashankaraiah, G. S. Suresh, T.V.Venkatesha, *Journal of The Electrochemical Society*, 2012,159 (7) A1-A8

16 X. Han, C. Chang, L. Yuan, T. Sun and J. Sun, *Adv.Mater.,* 2007, **19**, 1616.

17 K. Liu, J. Zheng, G. Zhong and Y. Yang, *J.Mater.Chem.,* 2011, **21**, 4125.

18 M. D. Levi, D. Aurbach, *J.Electroanalytical Chemistry*, 1997, **421**, 79-88.

19 Z. Song, H. Zhan and Y. Zhou, *Chem. Commun.*, 2009, **448**-450.

20 T. Le Gall, K. H. Reiman, M. C. Grossel and J. R. Owen, *J. Power Sources.*,2003, **119**, 316.

View Article Online
DOI: 10.1039/C5NJ01300C

21 H.Wang, K. Huang, Y. Zeng, F. Zhao and L.Chen, *Electrochemical and solid state letters.,* 2007, **10**, A199-A203.

22 K. Hansen, K. West, *Electrochemical Society Proceedings*, 1997, **18.**

23 C. Luo, Y. Zhu, Y. Xu, Y. Liu, T. Gao, J. Wang , C, Wang, *J. Power Sources.,*2014, **250** 372-378.

24 W. Tang, Y. Zhu, Y. Hou, L. Liu, Y. Wu, K. P. Loh, H. Zhangc, K. Zhud, *Energy Environ. Sci*., 2013, **6**, 2093.

25 A. Saxena, J. R. Celaya, I. Roychoudhury, S. Saha, B. Saha, K. Goebel, *European Conference of Prognostics and Health Management Society* 2012, 1-11.

26 Y. Wang, S. Chou, H. Liu, S. Dou, *Carbon* 2013, **57**, 202-208

27 J-W. Lee, S-I. I. Pyun, *Electrochim. Acta.,* 2004, **49**, 753-761.

28 N. N. Sinha, P. Ragupathy, H. N. Vasan, N. Munichandraiah, *Int. J. Electrochem.Soc.,* 2008, **3**, 691-710.

29 C. Ho, I. D. Raistrick, R. A. Huggins, *J.Electrochem.Soc.,* 1980, **127**, 343-350.

30 T. Pajkossy, T. Wandlowski, R.S. Neves, *J.Electroanal.Chem.,* 1996, **414**, 209.

View Article Online
DOI: 10.1039/C5NJ01300C

Figures with Caption:

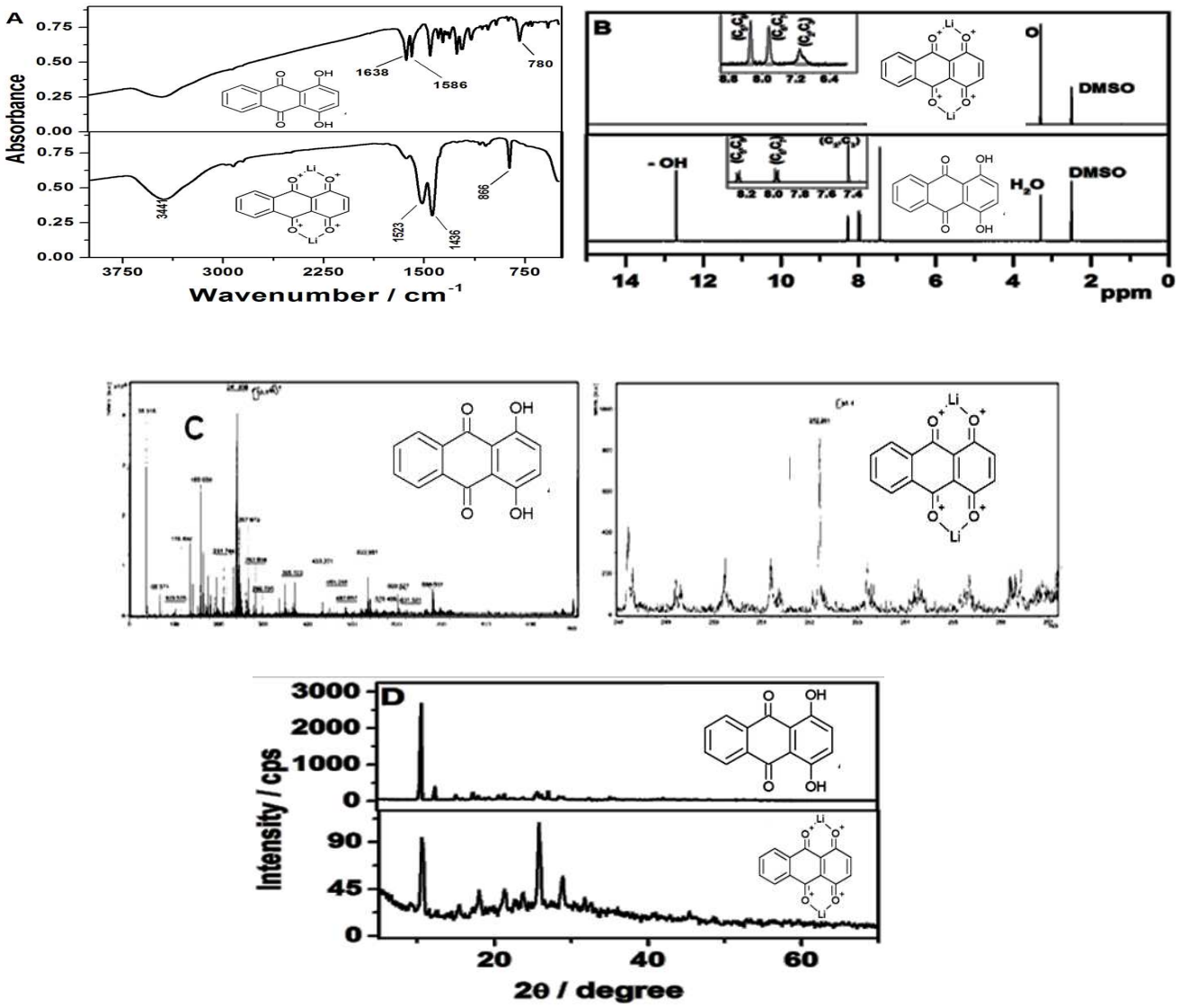

Fig. 1: A) FT-IR spectra, B) ^{1}H-NMR spectra, C) MALDI-TOF Maas spectra and D) pXRD patterns of quinizarin and Lithiated quinizarin.

View Article Online
DOI: 10.1039/C5NJ01300C

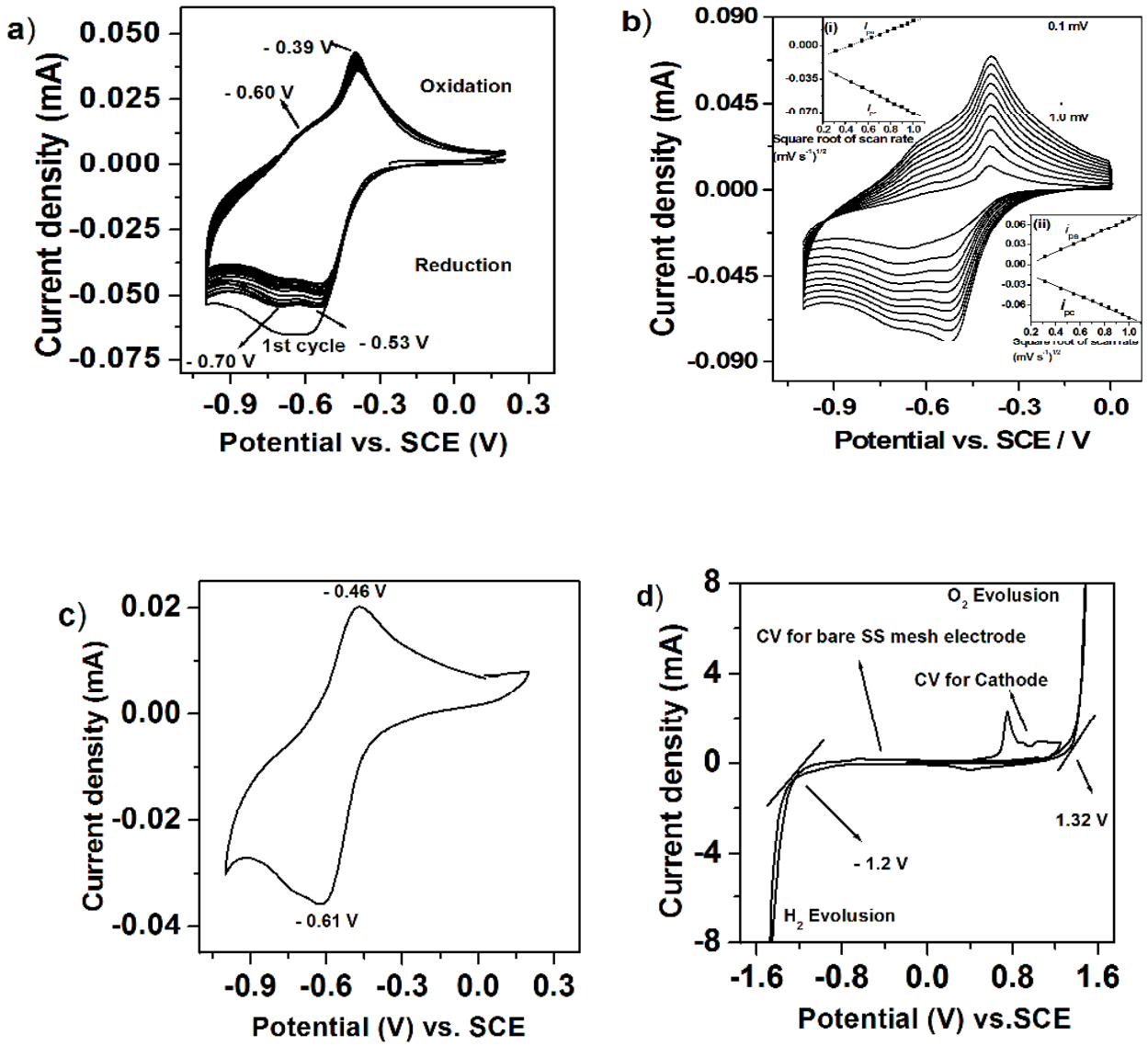

Fig. 2: Cyclic voltammograms of Lithiated quinizarin in saturated Li_2SO_4 solution a) at the potential scan rate of 0.5 mV s^{-1} for different cycles, b) at different scan rate from 0.1 mV s^{-1} to 1.0 mV s^{-1} Inset shows the relationship between the peak currents and square root of scan rate at different scan rates, c) at potential scan rate of 0.05 mV s^{-1}, d) bare SS electrode to show evolution of H_2 and O_2 gas in comparison with cathode

View Article Online
DOI: 10.1039/C5NJ01300C

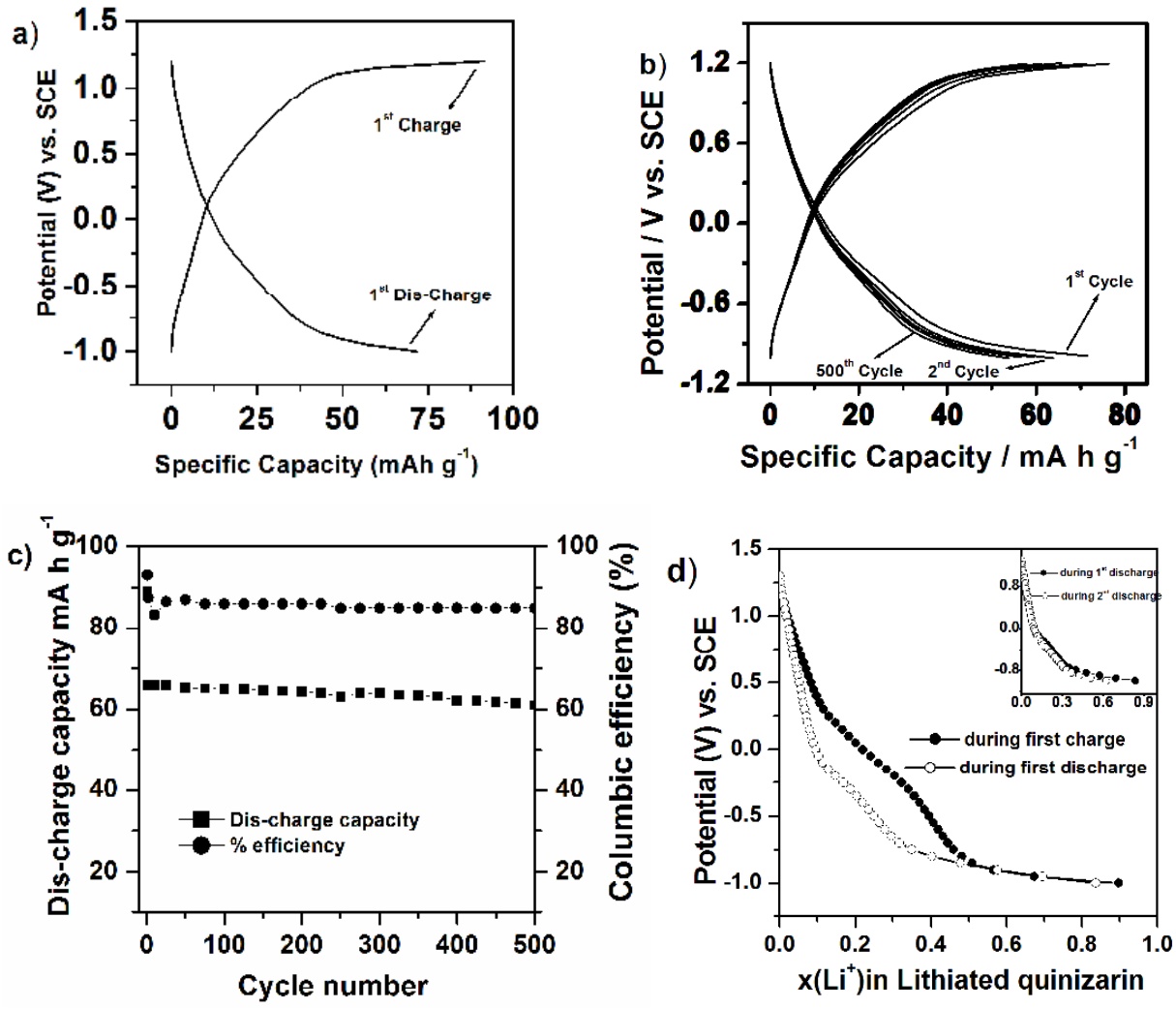

Fig. 3: Galvanostatic charge-discharge curves a) at C/10 rate for 500 cycles b) at different rates c) columbic efficiency of discharge capacity with cycle number d) x(Li^+) during charge/discharge.

View Article Online
DOI: 10.1039/C5NJ01300C

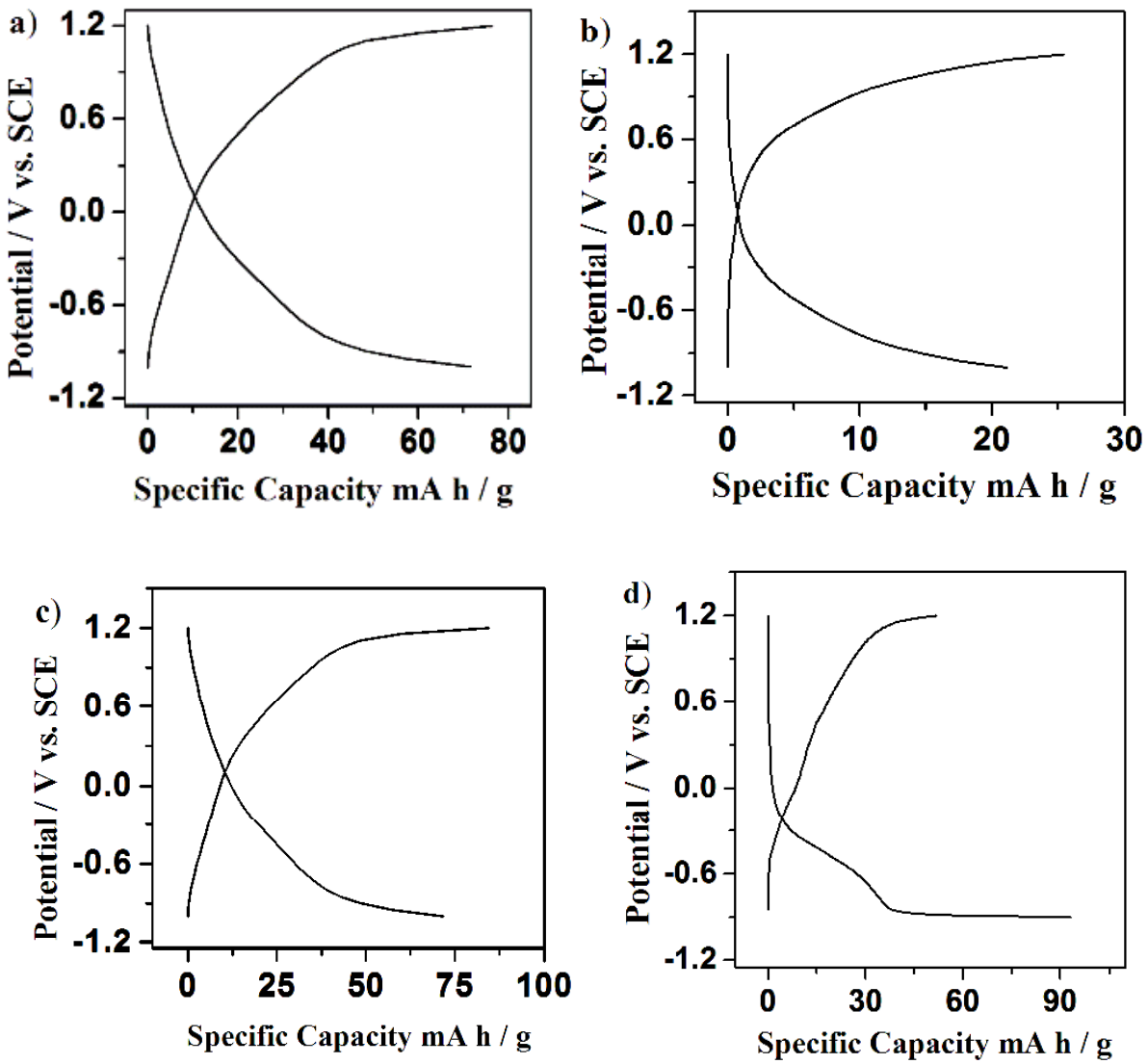

Fig. 4: Galvanostatic Charge discharge by using three electrode systems at different n/p ratio a) 1: 0.75 b) 1: 0.5 c) 1: 1 d) 0.75: 1

View Article Online
DOI: 10.1039/C5NJ01300C

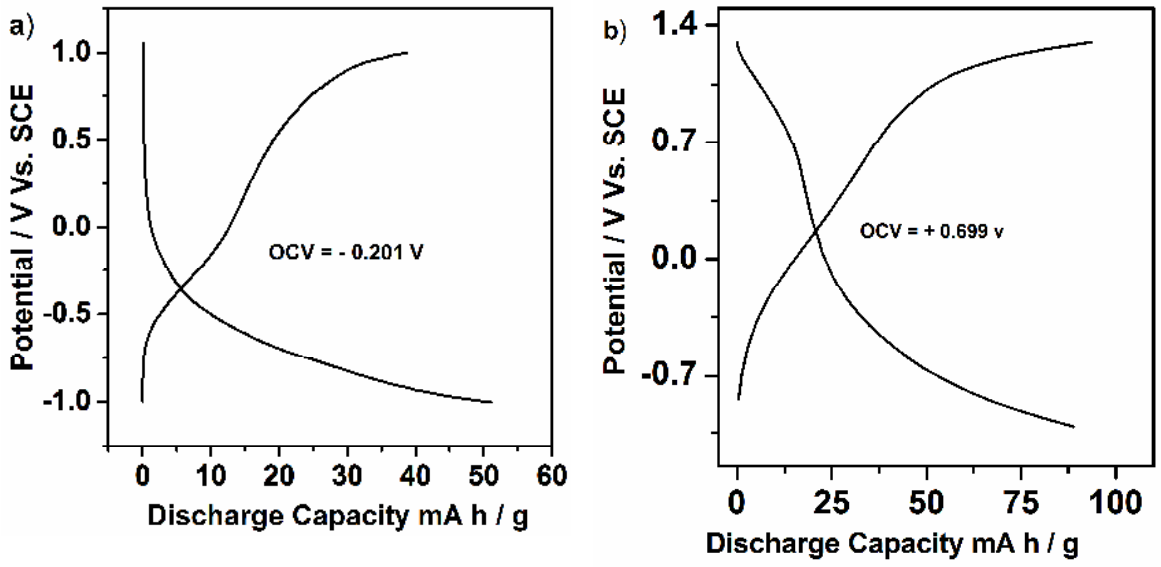

Fig. 5: Galvanostatic charge discharge profile to show the half cell potential of a) Lithiated quinizarin, b) $LiNi_{1/3}Co_{1/3}Mn_{1/3}O_2$ in aqueous saturated Li_2SO_4 solution.

View Article Online
DOI: 10.1039/C5NJ01300C

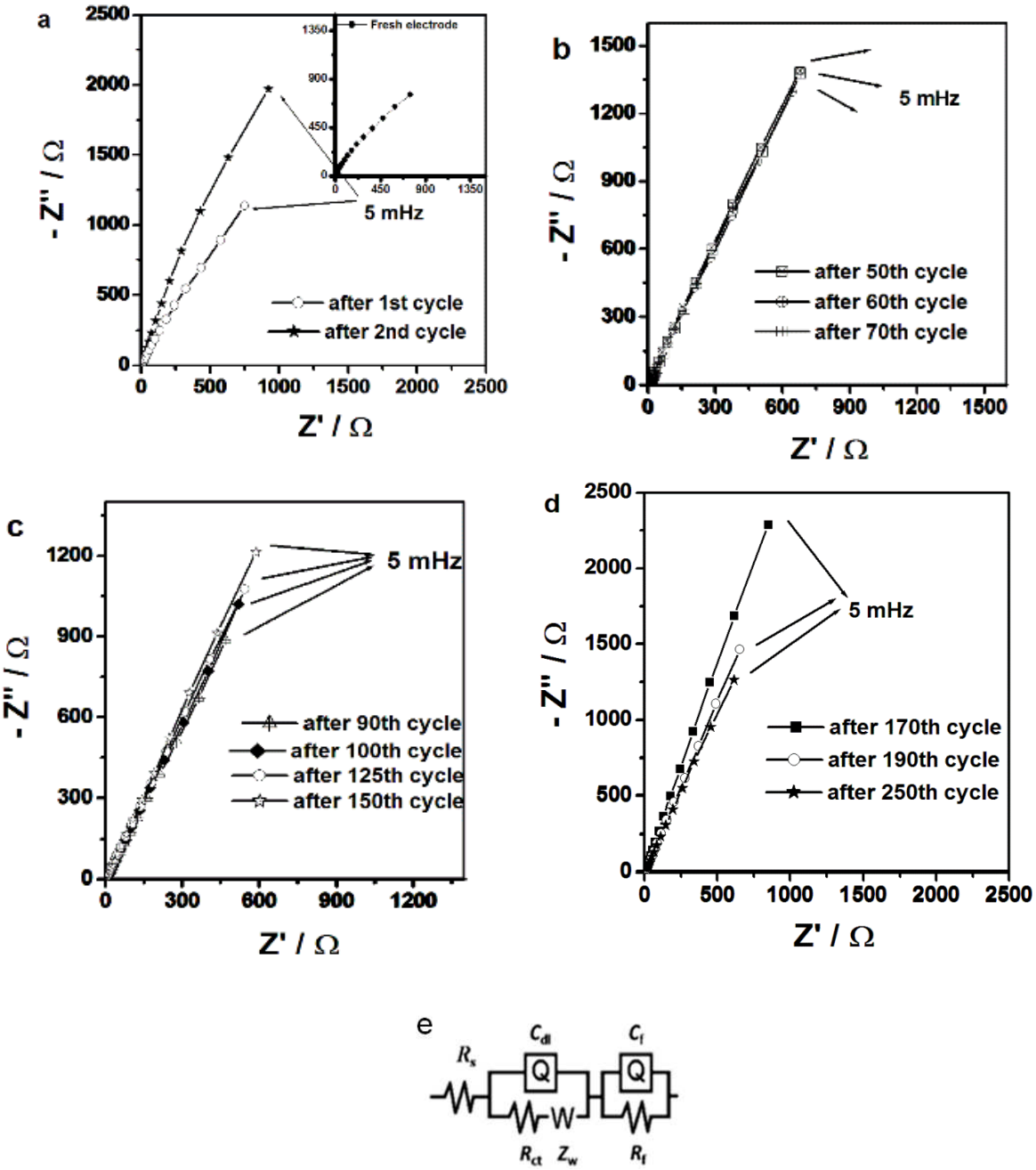

Fig. 6: Nyquist plots measured in sat.Li_2SO_4 solution at open circuit potential from a) to d) with fresh impedance from cycle 1 to 250. Simulation results obtained by the equivalent circuits (e)

View Article Online
DOI: 10.1039/C5NJ01300C

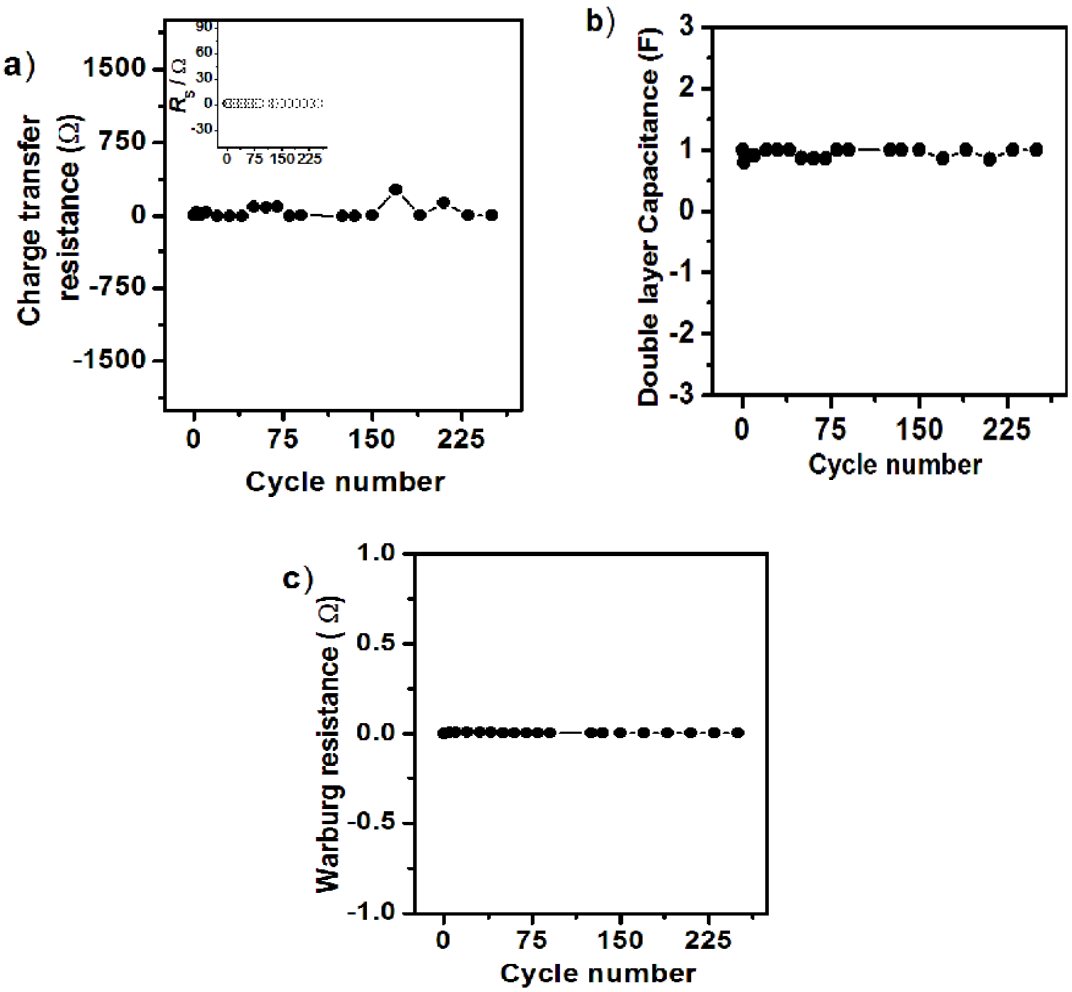

Fig. 7: Relationship between a) charge transfer resistance and solution resistance, b) double layer capacitance and c) Warburg resistance with CVcycle numbers at a scan rate of 0.5 mV/sec.

View Article Online
DOI: 10.1039/C5NJ01300C

Graphical Abstract:

An appreciable average voltage and discharge capacity of an aqueous cell was achieved by a lithiated organic electroactive species called quinizarin synthesised by ultrasonic method.